

MONTE CARLO SIMULATION OF DEFORMATION SUBSTRUCTURE EVOLUTION DURING RECRYSTALLIZATION*

B. Radhakrishnan, G. Sarma and T. Zacharia
Oak Ridge National Laboratory
P.O. Box 2008, MS-6140, Oak Ridge, TN 37831-6140, USA

Introduction

Recently [1,2], a microstructure and texture evolution model was presented for static recrystallization by coupling a Monte Carlo (MC) simulation of recrystallization with a finite element (FE) simulation of microstructural deformation based on crystal plasticity. The crystal plasticity model provided a quantitative description of the orientation distributions in the deformed microstructure. This allowed the rigorous representation of the crystallographic orientations in the deformed microstructure in the form of axis-angle pairs in the MC simulations rather than by orientation numbers as in the past [3-6]. The crystal plasticity model also provided a quantitative description of the stored energy of deformation at each MC site, which, together with the orientation information, allowed the incorporation of a nucleation model for recrystallization. Hence, it was possible to predict the spatial distribution and orientations of nuclei and their dependence on the amount of prior deformation.

However, in the above model, recrystallization was represented as a two-step process involving distinct nucleation and growth stages, similar to the classic diffusional phase transformations. This is because of the general observation that recrystallization is characterized by the presence of an incubation phase during which many locations in the deformed microstructure “nucleate” strain-free grains generally bounded by high-angle boundaries, followed by a growth phase in which these boundaries sweep through the deformed microstructure. However, it is known that the mechanism of nucleation during recrystallization is different from that in phase transformations in that the nuclei either already exist in the deformed microstructure in the form of supercritical subgrains/cells or they form by the heterogeneous growth of pre-existing subcells/grains [7,8] in the deformation substructure. The growth phase simply involves the continued heterogeneous movement of the nuclei boundaries into the not yet evolved regions of the substructure.

In this paper, a new model for recrystallization is presented where recrystallization is modeled as a one-step, heterogeneous subgrain growth process. The simulations indicate how existing prior high angle boundaries as well as the high angle boundaries produced by the deformation process migrate to sweep through the deformed regions to produce typical recrystallized microstructures and kinetics. The simulations also capture the heterogeneous growth of subgrains induced by long-range orientation gradients present in the deformation substructure. The simulations are used to evaluate the recrystallization kinetics, microstructure and texture evolution for deformed fcc polycrystals.

*The submitted manuscript has been authored by a contractor of the U.S. Government under contract No. DE-AC05-96OR22464. Accordingly, the U.S. Government retains a non-exclusive, royalty-free license to publish or reproduce the published form of this contribution, or allow others to do so, for U.S. Government purposes.

Computational Approach

The computational approach is similar to the one used previously [1,2]. The crystal plasticity FE model, and its application to the deformation of grain structures is described elsewhere [9]. The unique feature of the FE simulations is that it captures the heterogeneity of deformation at the scale of the microstructure and provides a quantitative description of the stored energy, plastic strain and crystallographic orientation in the deformed microstructure. The above information is mapped from the distorted FE mesh to a regular, cubic mesh by using a procedure described elsewhere [2]. The deformation substructure at each grid point is then obtained from the stored energy per unit volume at the site provided by the FE calculations. Each grid site is assumed to consist of a subgrain network with a mean subgrain size. The stored energy per unit volume at a site with coordinates i , j , and k , H_{ijk} , is assumed to be equal to the surface energy per unit volume of the subgrain network given by [10],

$$H_{ijk} = \frac{2\gamma_{ijk}}{D_{ijk}}, \quad (1)$$

where D_{ijk} is the mean subgrain size and γ_{ijk} is the specific boundary energy of a subgrain given by

$$\gamma_{ijk} = \begin{cases} \gamma_m \frac{\theta}{\theta^*} \left[1 - \ln \left(\frac{\theta}{\theta^*} \right) \right] & \text{when } \theta \leq \theta^*, \\ \gamma_m & \text{when } \theta > \theta^*, \end{cases} \quad (2)$$

where θ is the mean misorientation between subgrains at the site, γ_m is the specific energy of a high-angle boundary, and θ^* is the misorientation limit for low angle boundaries, which is usually taken as 15° . The above equations are used to calculate the mean misorientation between subgrains at every site, assuming that the mean subgrain size is the same for all sites. The calculations result in a local sublattice for each site in the form of a subgrain network that is characterized by a known mean subgrain size and a mean misorientation between subgrains. These sublattices are assembled to generate a global MC lattice that contains the deformation substructure for the entire volume.

The evolution during subsequent annealing of the above subgrain network that represents the deformation substructure is simulated by using a Monte Carlo technique. In the MC simulations, each MC site is visited in a random fashion and the local energy of the site and its neighborhood, E_{init} , is calculated using,

$$E_{init} = \sum_i \gamma_i, \quad (3)$$

where γ_i is the specific boundary energy between the site and its i^{th} neighbor. γ_i is a function of the misorientation between the two sites, as in equation (2). The misorientation, θ , is calculated using the axis-angle pairs for the two sites [9]. The energy of the site and its neighborhood when the site is replaced by one of its nearest neighbors, E_{fin} is then calculated as,

$$E_{fin} = \sum_i \gamma'_i, \quad (4)$$

where γ'_i is the orientation dependent specific boundary energy between the replaced neighboring orientation and the original neighborhood of the site. The local energy change ΔE is calculated as $E_{fin} - E_{init}$. The probability of flipping the site to the orientation of the chosen nearest neighbor, p , is calculated as,

$$p = \begin{cases} k' & \Delta E \leq 0 \\ k' \exp(-\Delta E/kT) & \Delta E > 0 \end{cases} \quad (5)$$

where k is Boltzmann's constant and k' is the misorientation-dependent boundary mobility given by [11]

$$k' = [1 - \exp(-q\theta^3)], \quad (6)$$

where q is a constant, assumed to be 0.001 in the current simulations. In equation (5), the quantity kT is assumed to be equal to $0.4 \times \gamma_m$. It is important to note that T here is not the actual temperature but the lattice temperature used in MC simulations. The reorientation of the site is implemented with the probability p calculated using equations (5) and (6).

Simulations

The computational approach described above was used to simulate the recrystallization kinetics, microstructure and texture evolution for plane strain deformations of 50% and 68%, respectively, by using the 12 octahedral $\{111\} \langle 110 \rangle$ fcc slip systems. The deformed microstructure in each case was first mapped to a $30 \times 30 \times 30$ regular cubic grid. In order to obtain a statistical representation of the subgrain network for each site, a reasonable sublattice size for each site is $15 \times 15 \times 15$, with a subgrain size 1/15 the site size. The overall size of the MC mesh in this case becomes $450 \times 450 \times 450$. However, this problem size is too large for single processor workstations. Hence, it was decided to carry out the recrystallization simulations in two-dimensions by taking 30×30 sections of the $30 \times 30 \times 30$ lattice and using a sublattice size of 15×15 for each site. In the current recrystallization simulations, the results for the midsection containing the rolling and normal directions are presented. The MC grid size of 450×450 is easily handled by single processor workstations. However, work is underway to implement the recrystallization simulation on a parallel computing platform, so that a full three-dimensional simulation can be carried out.

Results and Discussion

Fig. 1(a) shows the expected positions of prior grain boundaries in the 50% deformed microstructure, assuming that the deformation occurs uniformly throughout the microstructure. Fig. 1(b) shows the deformed microstructure for the same section obtained by the FE simulation, showing the locations of boundaries with misorientations greater than or equal to 15° . It is clear that the inhomogeneous deformation at the scale of the microstructure has resulted in the formation of several high angle boundary segments, in addition to the original high angle grain boundaries that survive the deformation process. Extensive investigations of deformation substructures by transmission electron microscopy [12] have revealed that such strain localization and local variations in strain path do result in the formation of deformation induced high angle boundaries. The

high angle boundaries formed by the deformation process, as well as some segments of the initial high angle boundaries, are potential sites for where heterogeneous subgrain growth is triggered.

The temporal evolution of the recrystallization process is shown in Fig. 2 for the deformed grain structure of Fig. 1(b). The high angle and low angle boundaries (misorientation $< 15^\circ$) are indicated by dark and light lines, respectively. The discontinuous subgrain growth originating at the high angle boundaries results in the sweeping of the deformed microstructure by the migrating high angle boundaries, thus simulating recrystallization. In regions where high angle boundaries do not exist, discontinuous growth of subgrains occurs when certain subgrains gain a growth advantage over the neighboring subgrains, probably induced by a long range orientation gradient. Such a discontinuous growth can ultimately lead to the formation of a high angle boundary. However, it is important to note that the recrystallized microstructure contains both high angle and low angle boundaries. The unique feature of the recrystallization simulation is that it is not necessary to invoke a separate nucleation model as was done in a previous study [6]. All the potential nucleation mechanisms operate automatically depending upon the local substructure. Fig. 3 shows the recrystallized microstructure after a Monte Carlo Step (MCS) of 500 for initial deformations of 50% and 68%, respectively. Note that higher prior deformation leads to a finer recrystallized grain size. In Fig. 3(a), the recrystallization is not complete since regions with a fine substructure are still present. However, such regions are almost absent in Fig. 3(b) indicating complete recrystallization. This is due to the more uniform distribution of deformation induced high angle boundaries in the latter case.

The recrystallization kinetics are shown in Fig. 4. The variation of recrystallized volume fraction with time shown in Fig. 4(a) has the typically observed sigmoidal kinetics of recrystallization. Fig. 4(b) shows that the recrystallization kinetics exhibits significant deviations from ideal Johnson-Mehl-Avrami-Kolmogorov (JMAK) kinetics [10], probably because of the non-random distribution of nucleating sites and anisotropic growth of the nucleation fronts. Prior deformation of 68% has clearly resulted in a significant acceleration of the recrystallization kinetics compared to the kinetics for a prior deformation of 50%. This is due to the higher stored energy in the former case which results in greater misorientation between subgrains in the deformed microstructure, leading to a greater mobility of the subgrain boundaries.

In addition to the microstructural and kinetics effects described above, the current simulations also capture the evolution of the recrystallization texture. Fig. 5 shows the $\langle 100 \rangle$ pole figures of the deformation and recrystallization textures for the 68% deformation case. The deformation texture consists of brass, S and copper components commonly seen in deformed fcc materials. The recrystallization texture shows the redistribution of the intensities of the deformation texture components due to the preferential growth of certain subgrains at the expense of the others. Of particular significance is the strengthening of the RD rotated cube component present in the deformation substructure.

Conclusions

The recrystallization of fcc polycrystals has been simulated with a technique that couples FE simulation of microstructural deformation with a novel MC technique that treats recrystallization as a heterogeneous subgrain growth process. The recrystallization simulation captures nucleation by heterogeneous subgrain growth, and deformation-induced formation of high angle boundaries, as well as the growth of the nuclei by sweeping through the deformation substructure. The observed recrystallization kinetics and microstructure, and their variation with extent of prior deformation are in agreement with general experimental observations. The model is also able to capture the evolution of recrystallization textures.

Acknowledgments

This research was sponsored by the Office of Basic Energy Sciences, U.S. Department of Energy, under contract DE-AC05-96OR22464 with Lockheed Martin Energy Research Corporation. The research was supported in part by an appointment to the Oak Ridge National Laboratory Postdoctoral Research Associates Program administered jointly by the Oak Ridge National Laboratory and the Oak Ridge Institute for Science and Education. The authors acknowledge the use of the Intel Paragon XP/S 35 located in the Oak Ridge National Laboratory Center for Computational Sciences (CCS), funded by the Department of Energy's Office of Scientific Computing.

References

1. G. Sarma, B. Radhakrishnan and T. Zacharia, Proc. ReX' 96, The Third Int. Conf. on Recrystallization and Related Phenomena, Monterey, CA, 555 (1997).
2. B. Radhakrishnan, G. Sarma and T. Zacharia, Acta mater., to appear.
3. D.J. Srolovitz, G.S. Grest and M.P. Anderson, Acta metall., 34, 1833 (1986).
4. D.J. Srolovitz et al., Acta metall., 36, 2115 (1988).
5. A.D. Rollett et al., Acta Metall., 40, 3475 (1992).
6. A.D. Rollett et al., Acta metall., 37, 627 (1989).
7. R.D. Doherty et al., Proc. of the 16th Risø Int. Symp. on Materials Science: Microstructural and Crystallographic Aspects of Recrystallization, Roskilde, Denmark, 1 (1995).
8. F.J. Humphreys, Acta. mater., 45, 4231 (1997).
9. G. Sarma, B. Radhakrishnan and T. Zacharia, submitted to Computational Materials Science.
10. F.J. Humphreys and M. Hatherly, Recrystallization and Related Annealing Phenomena, Oxford, U.K., (1995).
11. A.D. Rollett and E.A. Holm, Proc. ReX' 96, The Third Int. Conf. on Recrystallization and Related Phenomena, Monterey, CA, 31 (1997).
12. D.A. Hughes, Acta. mater., 45, 3871 (1997).

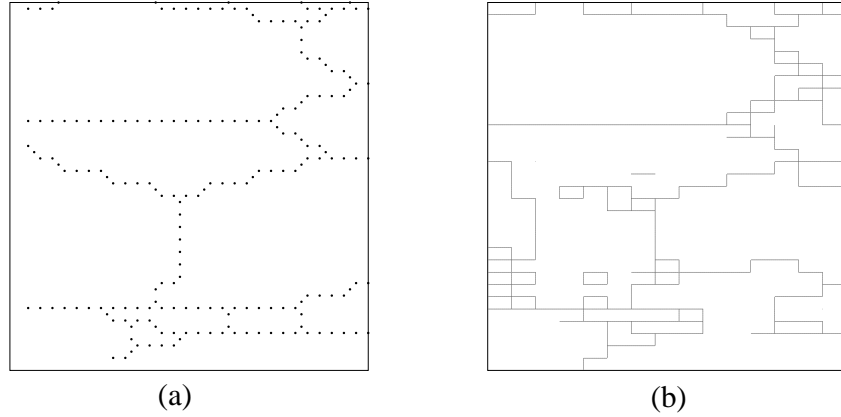


Figure 1: Deformed grain structures after 50% deformation (a) assuming uniform deformation and (b) FE results.

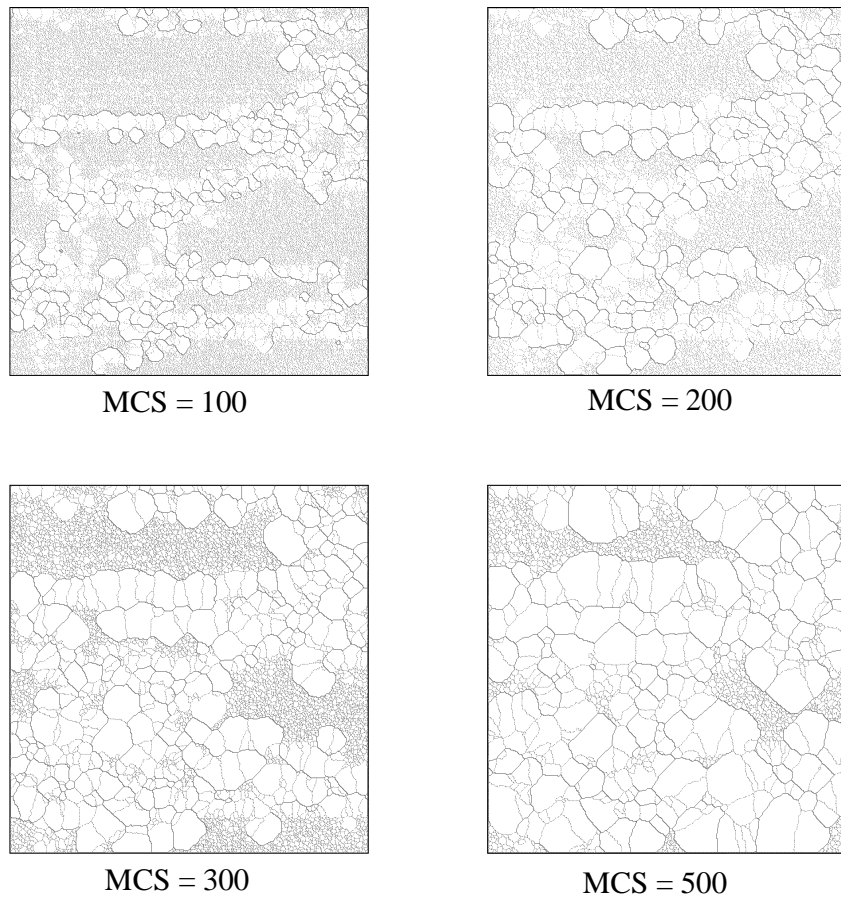


Figure 2: Temporal evolution of recrystallized microstructure for the deformed microstructure shown in Fig. 1.

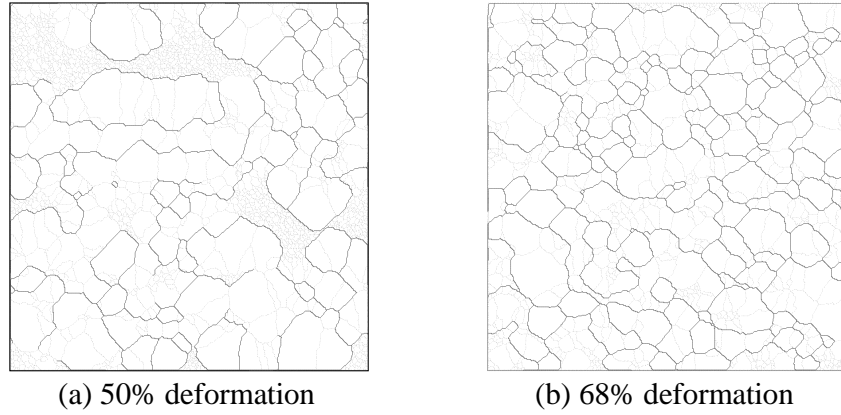


Figure 3: Effect of amount of prior deformation on recrystallized microstructure at MCS=500.

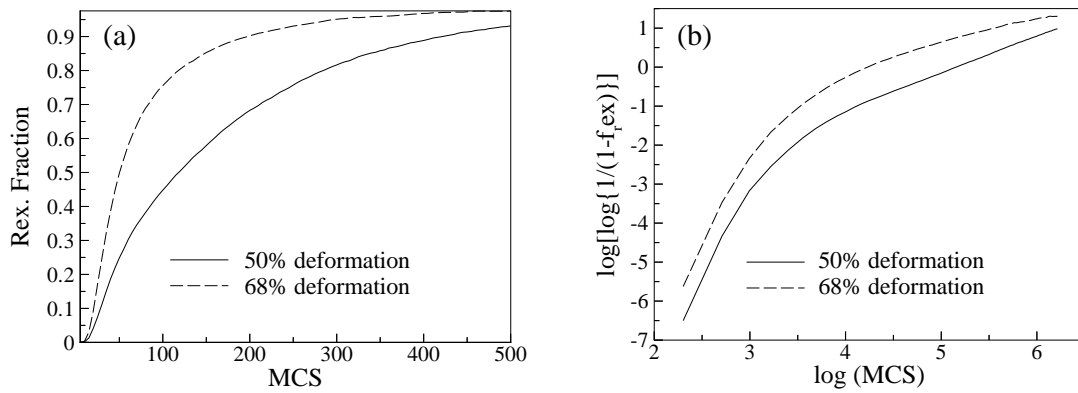


Figure 4: Effect of amount of prior deformation on recrystallization kinetics. (a) Recrystallized volume fraction vs. MCS. (b) JMAK plot.

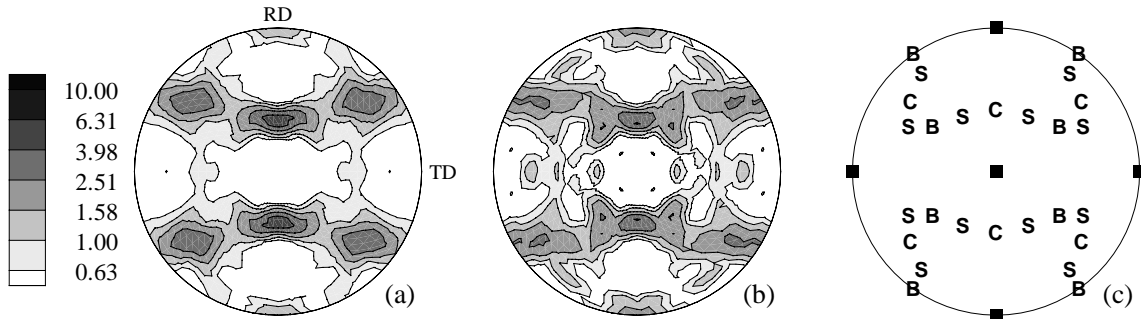


Figure 5: Deformation (a) and recrystallization (b) textures for a prior deformation of 68 %. (c) Ideal orientations of texture components commonly observed for deformed fcc polycrystals (B: Brass, C: copper, S: S, square: cube)